ELSEVIER

Journal of Electron Spectroscopy and Related Phenomena 88–91 (1998) 1015–1020

JOURNAL OF ELECTRON SPECTROSCOPY and Related Phenomena

High-resolution photoemission combined with low-temperature STM

H. Hövel[a], T. Becker[b], D. Funnemann[b], B. Grimm[a], C. Quitmann[a], B. Reihl[a,*]

[a]*University of Dortmund, Experimentelle Physik I, D-44221 Dortmund, Germany*
[b]*OMICRON Vakuumphysik GmbH, D-65232 Taunusstein, Germany*

Abstract

A novel low-temperature (LT) surface-science facility based on a two-chamber UHV system has been developed for combined investigations of the electronic and geometric structure of surfaces, employing scanning tunneling microscopy at $T \leq 5$ K and high-resolution ($\Delta E \cong 10$ meV) photoemission at $T \leq 50$ K. A LHe-cooled sample manipulator enables cold transfer of samples (and tips) between the two chambers. Here we present the LT-UHV facility together with first measurements on silver surfaces and silver clusters prepared in nanopits of a graphite surface. © 1998 Elsevier Science B.V.

Keywords: High-resolution photoemission; Scanning Tunneling Microscopy; Low Temperatures; Cluster formation

1. Introduction

We have built a novel low-temperature (LT) surface-science facility based on a two-chamber ultra-high vacuum (UHV) system connected by a LHe-cooled sample manipulator which enables cold transfer of samples (and tips) between the two chambers. One of them contains the LT scanning tunneling microscope (STM) with proven atomic resolution at $T \leq 5$ K, the other chamber carries the high-resolution (HR) photoelectron analyzer together with sample preparation (evaporation, sputter-cleaning, heating) and characterization (LEED, Auger) techniques. Such a combination of measurement techniques provides the optimum way to perform a 'complete' surface-science experiment and study both, the electronic and geometric properties of a specimen surface as well as their interdependencies. Here we describe the UHV facility together with the LT STM and the high-resolution analyzer, and present first measurements on silver surfaces and silver clusters prepared in nanopits of a graphite surface.

Low temperature phenomena like, for example, magnetism, superconductivity, structural phase transitions, charge and spin density waves, metal–insulator transitions, etc., are typical bulk phenomena occurring below characteristic transition temperatures which often fall near the absolute zero temperature. Small variations in temperature can have drastic effects, if T changes through such a transition temperature. But even without a transition temperature nearby, changes in temperature often enter through an exponential of ($\pm k_B T$) or T^n power dependence, thus strongly enhancing temperature phenomena.

In surface and interface science T-dependent bulk phenomena persist, but the surface acts as yet another 'disturbance' with new or different T-dependencies. For instance, magnetic transition temperatures may differ at the surface from the bulk values, or superconductivity may vanish completely at the surface/interface of a specimen. Additional T-dependent effects exist at interfaces or on surfaces: surface

* Corresponding author. Tel: +49-231-755-3506; Fax: +49-231-755-3657; Email: reihl@physik.uni-dortmund.de.

PII S0368-2048(97)00114-X

reconstruction, growth mechanisms (cluster formation, island growth, stability and size effects), surface metallization, gas adsorption, etc.

For a complete understanding of most effects, it is important to obtain information on both, the electronic and geometric structure and understand their inter-dependencies. Ultraviolet photoelectron spectroscopy (UPS) suffers from phonon broadening at room temperature [1], which can however be reduced by cooling the specimen. Thus, complex multiplet splittings and surface core-level shifts may be resolved (compare the original cerium data [2] to the recent HR work [3], or the first heavy-fermion spectrum [4] to the HR data [5]). Of course, temperature effects like an antiferromagnetic transition at 33 K and its influence on the band structure [6], the incommensurate–commensurate transition of the charge-density wave in TaS_2 [7], the opening of the superconducting gap in high-T_c superconductors [8], or the screening properties of Xe films adsorbed at 30 K [9] require adequate energy resolution which in extreme cases must be below 5 meV.

Scanning tunneling microscopy (STM) itself is well suited to study geometric and electronic properties of surfaces. Due to its scanning action, however, STM is a relatively slow probe. By cooling, phenomena like diffusion and corrosion can sufficiently be slowed down so that they become accessible by scanning probe techniques. Since vibrational and rotational movements of single atoms and molecules are also frozen in with cooling, STM topographic picture often appear crisper at lower T. In cases where the signal-to-noise ratio is poor in an STM experiment, increasing the tunneling current can often help. This, however, is limited by thermal heating and eventually destroys the STM tip. At LT, tunneling currents reach well into the μA-range, hence improving signals which are proportional to it.

The best characterized environment for STM is UHV, also at low temperatures. Eigler and Schweizer [10] were the first to successfully build a UHV LT STM. Manipulation of single xenon atoms on Ni(110) at 4 K and the visualization of the standing electron waves of a surface state on Cu(111) are just two examples of Eigler et al.'s spectacular results [10,11].

A first successful set-up of a low-temperature UHV STM with the full in-situ flexibility of tip and sample exchange at 5 K was realized at the IBM Zurich Research Laboratory [12]. Experience showed, however, that certain improvements of that design [12] would greatly enhance the performance of the UHV STM at low temperatures, hence a novel LT STM solution was developed (for more details see ref. [13]). Its three-dimensional x-y-z coarse approach allows to reach any point on the sample surface within a 5×5 mm^2 square, and its vibrational isolation via spring suspension and eddy-current damping is optimal against acoustic and mechanical vibrations. This novel design was able to routinely produce [13] atomically resolved STM topographs at $T = 5$ K of Au(111), Si(111)7 $\times$ 7, and visualize the charge density waves on $NbSe_2$(111).

2. Experimental

The fast tip and sample exchange of the LT STM at 5 K with thermal equilibrium conditions reached again after less than 1 h suggests to combine it in a system solution with standardized surface-science techniques as simple attachments. We designed and built such an apparatus containing the new LT STM in one UHV chamber (see A in Fig. 1), and an energy analyzer (B) together with LEED (C), Auger electron

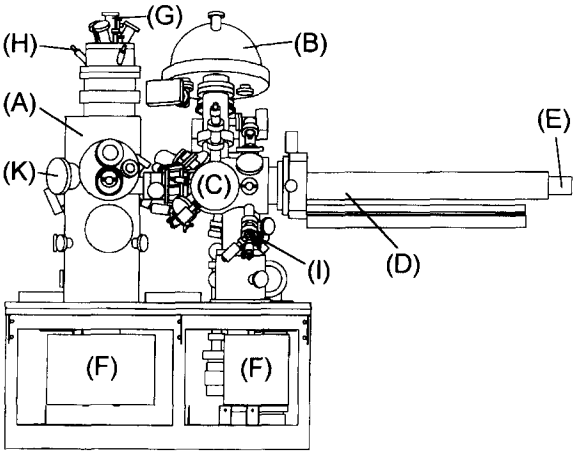

Fig. 1. Side view of the low-temperature surface science facility with the cryogenic set-up of the LT STM in the left chamber and the high-resolution photoelectron analyzer attached to the right chamber, which also contains LEED, Auger, ion-sputtering, and evaporation sources. The chambers are connected by a LHe-cooled sample translator for tip and sample transfer. See text for an explanation of the letters.

spectroscopy, ion-sputtering, evaporation, and a helium discharge lamp in the other UHV chamber. Both chambers are connected by an x-y-z sample translator (D) [14] with fast-load lock for sample introduction. A custom-built LHe flow cryostat (E) provides cooling capabilities to the sample translator with full 360° of rotation. The two main chambers are pumped by ion-getter and Ti-sublimation pumps (F) to base pressures in the 10^{-11} mbar range. The cryostat chamber contains the liquid-helium (LHe) bath cryostat (G) surrounded by a liquid-nitrogen (LN2) dewar (H) (see ref. [13] for a detailed sketch). In the preparation chamber, tips and samples can be heated and sputter-cleaned as well as be exposed to various evaporation sources (I) and gases. They can then be put inside a storage carousel (K) in the cryostat chamber, which is cooled to LN2 temperatures. On the sample translator tip and sample can be cooled to 40 K prior to their insertion into the STM head. For special UPS purposes, samples may be mounted on the heat exchanger of the translator, which reaches $T \leq 10$ K as measured by a Si diode.

3. Results and discussion

To check the performance of the LT STM we have measured [13] a well-ordered gold (111) surface with a $23 \times \sqrt{3}$ reconstruction and routinely obtained atomic resolved STM topographs at 5 K (not shown here, but in ref. [13]). An STM image from a surface with such a small corrugation of $\Delta z = 0.02$ nm is a very stringent test of the performance of the STM and the efficiency of the vibrational damping. The Au(111)$23 \times \sqrt{3}$ reconstructed surface with atoms separated by 0.288 nm was also used for the calibration of the piezos at the various temperatures and in particular at 5 K.

The UPS test of the HR photoelectron energy analyzer was performed on a sputter-cleaned silver film cooled to 10 K, employing HeI radiation ($h\nu$ = 21.2 eV). The pass energy of the analyzer was set to 0.7 eV. The photoemission spectrum with a width of 100 meV straddling the Fermi energy E_F is shown in Fig. 2. The energy resolution ΔE is derived [1] from the intersections of the 84% and 16% values of the total Fermi-level onset, corresponding to a $3.34kT$-width of the Fermi–Dirac distribution (cf. Fig. 2). The 50% value defines $E_F = 0$. In this way we arrive at $\Delta E = 10$ meV for the analyzer, which at these sample temperatures is entirely governed by the experimental energy resolution. Even with these extreme parameters, the total measurement time of this spectrum was only 30 min due to the parallel detection with an array of five channeltrons.

By sputtering and subsequent heating in on oxygen atmosphere, well-defined nanopits can be generated on HOPG (graphite) surfaces, which then may serve

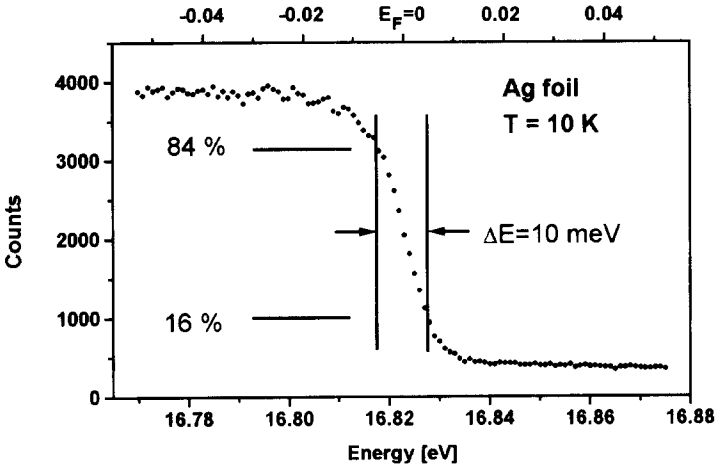

Fig. 2. Energy distribution curve of photoelectrons excited by HeI radiation ($h\nu$ = 21.2 eV) of a sputter-cleaned silver film at 10 K (pass energy 0.7 eV). The 84–16% difference of the Fermi-level onset provides the total energy resolution resulting in ΔE = 10 meV. The bottom abscissa gives the kinetic energy as measured, while the top abscissa is referred to $E_F = 0$ as derived from the 50% value of the onset.

as coagulation centers for the growth of metal clusters [15]. The goal is to measure their properties as a function of size and particle number. Only at low temperatures it was possible to resolve atomic structures also at the bottom of these pits, i.e. in the second layer of graphite and hence prove [15] that the nanopit was etched only one atomic layer deep. Fig. 3 shows an example of a graphite surface with a random distribution of nanopits of (9 ± 2) nm in diameter, measured with the LT STM at room temperature. The same surface after evaporation of 0.2 monolayers of silver, which has coagulated within the pits to form clusters with a rather homogeneous size distribution, is shown in Fig. 4. The distribution of cluster heights is determined to be (1.8 ± 0.5) nm.

In Fig. 5 we present the corresponding photoemission curves (taken at T = 40 K with $h\nu$ = 21.2 eV) of the graphite surface with nanopits (same surface as in Fig. 3) and covered with silver clusters (same surface as in Fig. 4). The data without clusters agrees well with photoemission results of the clean graphite (HOPG) in the literature. In other words, in contrast to STM, UPS does not reveal any signature of the nanopits present on the surface. The silver clusters, however, clearly show up also in UPS, particularly in the range between 4 and 7 eV below the Fermi level, where we expect the strong silver 4d emission to occur.

In order to identify the spectral contribution due to the silver clusters, we have taken the difference curve of the spectra of Fig. 5 and plotted it in Fig. 6 (upper curve). For comparison we have also measured the analogous spectrum of a thick silver film and show it as the lower curve in Fig. 6. We note that the spectral shape of the 4d-emission is different for the clusters, most probably due to the much bigger surface contribution in the case of clusters and a reduced coordination number [16]. The latter is known [17] to profoundly change the multiplet structure, since the convolution of the various spin-orbit split contributions appears like a broadening of the spectral features. Future data with better statistics will hopefully allow to make a fit and thus derive the contribution due to the different coordination numbers in the surface and in the bulk. Of course, the non-ideal homogeneous size distribution of the clusters must be improved, too.

The feature at −6.3 eV (see arrow in Fig. 6) on the other hand appears to be as sharp for the clusters as for the bulk film, in contrast to the broadened part of the 4d emission between 4 and 6 eV, where the bulk features are much sharper(see Fig. 6). This indicates

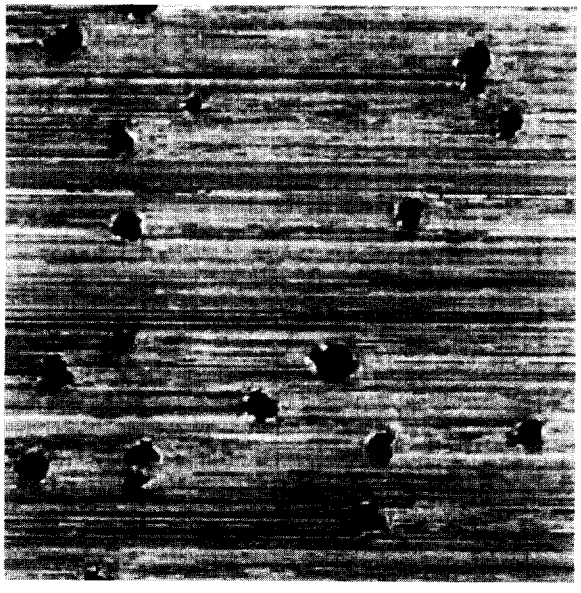

Fig. 3. Typical nanopit distribution produced in the HOPG surface as imaged by STM at 300 K. Parameters: $V_t = 0.29$ V; $I_t = 0.28$ nA; scan area 150 × 150 nm^2.

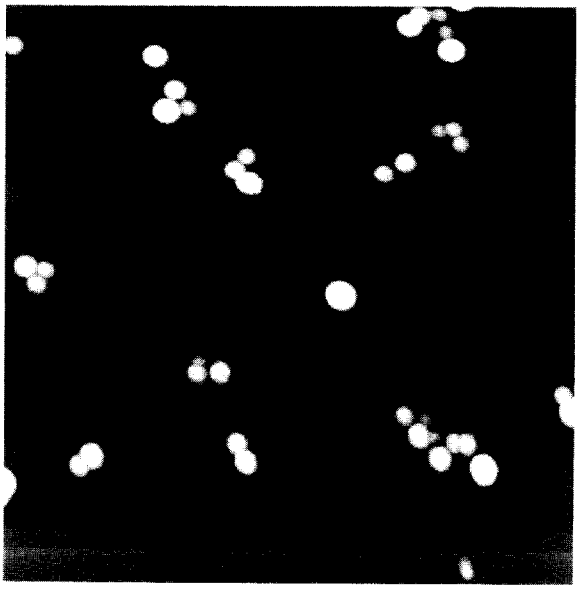

Fig. 4. STM image of the same sample surface as in Fig. 3, but now with silver clusters coagulated in the nanopits. Parameters: V_t = 0.97 V; I_t = 0.08 nA; scan area 150 × 150 nm^2.

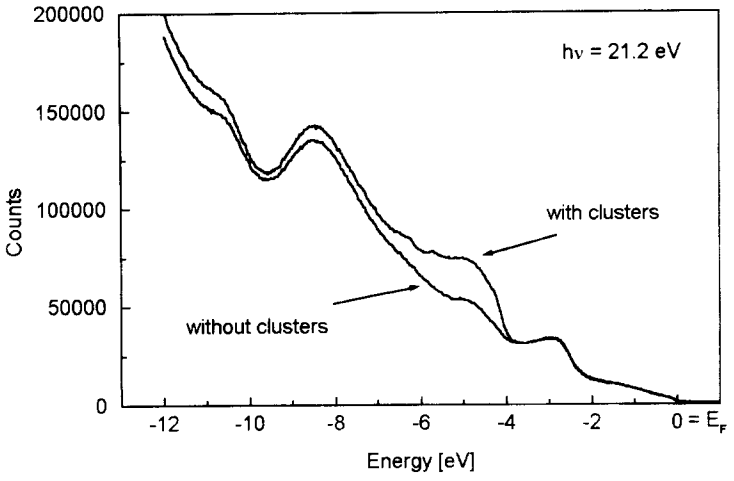

Fig. 5. Photoemission spectrum ($h\nu$ = 21.2 eV, pass energy 10 eV) of graphite with nanopits (lower curve) corresponding to the STM image of Fig. 3 and graphite with silver clusters (upper curve) corresponding to the STM image of Fig. 4 (substrate temperature T = 40 K).

that emission from atomic levels of the clusters may already show up at this cluster size. Cooling to 40 K has certainly helped to resolve this feature, since phonon broadening is already suppressed. Future I–V measurements with the LT STM on a single cluster will provide local information on the electronic structure and help clarify this interpretation. Such experiments performed with Pt clusters on graphite have proven to be very promising [18]. In this context it should also be noted that Freund and coworkers [19] have investigated the size-dependent shift of various core-level and valence-band peaks of clean and adsorbate-covered Rh, Pd, Ag, and Pt clusters. These shifts are discussed in terms of a size-dependent reactivity of the clusters.

In addition to the size-dependent changes of the electronic structure of the clusters, the photoelectron spectra are also influenced by the formation of an image charge in the final state. For clusters on a substrate the corresponding size-dependent energy-shift

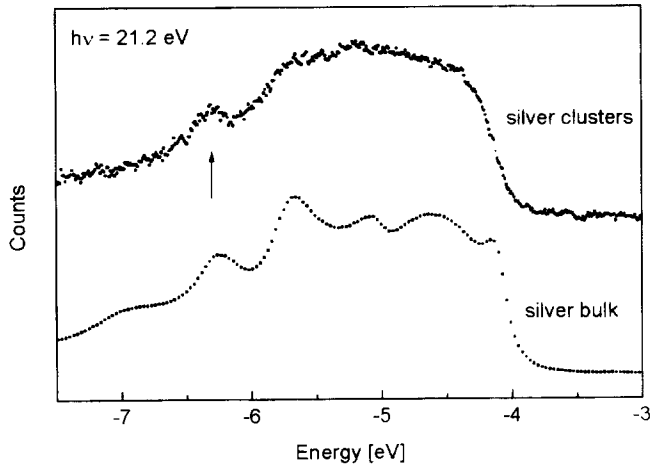

Fig. 6. Photoemission difference curve of Fig. 5 reflecting the 'pure' silver-cluster contribution in comparison to a spectrum with $h\nu$ = 21.2 eV of a clean silver film at T = 40 K (lower curve). Note the spectral feature at − 6.3 eV, see text. (The energy zero E_f = 0 is suppressed.)

of the whole spectrum is reduced compared to free clusters [20,21]. This may be utilized for a study of the cluster–substrate interaction. Here the use of high-resolution photoemission at low temperatures will allow to identify even small shifts.

4. Conclusions

The novel LT STM in combination with a high-resolution photoelectron analyzer provides means for the 'complete' surface science experiment, i.e. measuring the electronic and geometric structure as well as their interdependencies. As an example we have presented work on silver clusters in nanopits of graphite and referenced it to clean silver films. Distinct differences show up which need further investigations for a full understanding.

Acknowledgements

We thank R. Breil, G. Pike, M. Schaffhöfer, and F. Ströwer for their help with the sample preparation and the measurements.

References

[1] M. Cardona, L. Ley (Eds.), Photoemission in Solids, Springer-Verlag, Berlin, Heidelberg, New York, 1979.
[2] N. Mårtensson, B. Reihl, R.D. Parks, Solid State Commun. 41 (1982) 573.
[3] E. Weschke, C. Laubschat, T. Simmons, M. Domke, O. Strebel, G. Kaindl, Phys. Rev. B 44 (1991) 8304.
[4] G. Landgren, Y. Jugnet, J.F. Morar, A.J. Arko, Z. Fisk, J.L. Smith, H.R. Ott, B. Reihl, Phys. Rev. B 29 (1984) 320.
[5] A.J. Arko, J.J. Joyce, A.B. Andrews, J.D. Thompson, J.L. Smith, E. Moshopoulou, Z. Fisk, A.A. Menovsky, P.C. Canfield, C.G. Olson, Physica B 16 (1997) 230–232.
[6] B. Reihl, G. Hollinger, F.J. Himpsel, Phys. Rev B 28 (1983) 1490.
[7] R.A. Pollak, D.E. Eastman, F.J. Himpsel, P. Heimann, B. Reihl, Phys. Rev. B 24 (1981) 7435.
[8] Z.-X. Shen et al., Phys. Rev. Lett. 70 (1993) 1553.
[9] K. Horn, K.H. Frank, J.A. Wilder, B. Reihl, Phys. Rev. Lett. 57 (1986) 1064.
[10] D.M. Eigler, E.K. Schweizer, Nature 344 (1990) 524.
[11] M.F. Crommie, C.P. Lutz, D.M. Eigler, Nature 363 (1993) 524.
[12] R. Gaisch, J.K. Gimzewski, B. Reihl, R.R. Schlittler, M. Tschudy, W.D. Schneider, Ultramicroscopy 42-44 (1992) 1621.
[13] T. Becker, H. Hövel, M. Tschudy, B. Reihl, Appl. Phys. A, in press.
[14] Vacuum Generators, Hastings, England.
[15] H. Hövel, Th. Becker, A. Bettac, B. Reihl, M. Tschudy, E.J. Williams, J. Appl. Phys. 81 (1997) 154.
[16] G.K. Wertheim, S.B. DiCenzo, D.N.E. Buchanan, Phys. Rev. B 33 (1986) 5384.
[17] W.D. Schneider, C. Laubschat, B. Reihl, Phys. Rev. B 27 (1983) 6538.
[18] A. Bettac, V. Rank, K.-H. Meiwes Broer, submitted.
[19] H.J. Freund, Ang. Chem. Int. Ed. 36 (1997) 452 and references therein.
[20] G.K. Wertheim, Z. Phys. B 66 (1987) 53.
[21] K.H. Meiwes-Broer, Appl. Phys. A 55 (1992) 430.